Assessing the Distribution of Water Ice and Other Volatiles at the Lunar South Pole with LUVMI-X: A Mission Concept

Martin Losekamm, Janos Biswas, Thibaud Chupin, Michael Deiml, Matthieu Deremetz, Anthony Evagora, Guillaume Fau, Jessica Flahaut, Jeremi Gancet, Markus Glier, et al.

The Planetary Science Journal, 3:229 (14pp), 2022 October https://doi.org/10.3847/PSJ/ac8cfd

Assessing the Distribution of Water Ice and Other Volatiles at the Lunar South Pole with LUVMI-X: A Mission Concept

Martin J. Losekamm[1,2], Janos Biswas[3], Thibaud Chupin[4], Michael Deiml[5], Matthieu Deremetz[4], Anthony M. Evagora[6], Guillaume Fau[4], Jessica Flahaut[7], Jeremi Gancet[4], Markus Glier[5], Christian Gscheidle[3], Marine Joulaud[7,8], Hemanth K. Madakashira[4], Neil J. Murray[6], Jörg Neumann[9], Thomas Pöschl[1], Lutz Richter[5,10], Hannah M. Sargeant[11,13], Susanne Schröder[12], Jae Schwanethal[11], Simon Sheridan[11], Diego Urbina[4], David S. Vogt[12], and Peter Wessels[9]
[1] Technical University of Munich, Department of Physics, Garching, Germany
[2] Excellence Cluster ORIGINS, Garching, Germany; m.losekamm@tum.de
[3] Technical University of Munich, School of Engineering and Design, Garching, Germany
[4] Space Applications Services NV/SA, Sint-Stevens-Woluwe, Belgium
[5] OHB System AG, Wessling-Oberpfaffenhofen, Germany
[6] Dynamic Imaging Analytics Ltd., Milton Keynes, UK
[7] Centre de Recherche Pétrographiques et Géochimiques (CRPG), CNRS/Université de Lorraine, Vandoeuvre-lès-Nancy, France
[8] Now at Université Claude-Bernard Lyon 1, Lyon, France
[9] Laser Zentrum Hannover e.V., Hannover, Germany
[10] Now at LSS GmbH, Eching, Germany
[11] The Open University, School of Physical Sciences, Milton Keynes, UK
[12] German Aerospace Center, Institute of Optical Sensor Systems, Berlin, Germany
Received 2022 April 21; revised 2022 August 9; accepted 2022 August 24; published 2022 October 12

Abstract

The search for exploitable deposits of water and other volatiles at the Moon's poles has intensified considerably in recent years, due to the renewed strong interest in lunar exploration. With the return of humans to the lunar surface on the horizon, the use of locally available resources to support long-term and sustainable exploration programs, encompassing both robotic and crewed elements, has moved into focus of public and private actors alike. Our current knowledge about the distribution and concentration of water and other volatiles in the lunar rocks and regolith is, however, too limited to assess the feasibility and economic viability of resource-extraction efforts. On a more fundamental level, we currently lack sufficiently detailed data to fully understand the origins of lunar water and its migration to the polar regions. In this paper, we present LUVMI-X, a mission concept intended to address the shortage of in situ data on volatiles on the Moon that results from a recently concluded design study. Its central element is a compact rover equipped with complementary instrumentation capable of investigating both the surface and shallow subsurface of illuminated and shadowed areas at the lunar south pole. We describe the rover and instrument design, the mission's operational concept, and a preliminary landing-site analysis. We also discuss how LUVMI-X fits into the diverse landscape of lunar missions under development.

Unified Astronomy Thesaurus concepts: The Moon (1692); Lunar science (972); Lunar surface (974); Lunar mineralogy (962); Lunar craters (949); Cosmic rays (329); Solar radiation (1521); Space weather (2037); Lunar probes (969); Rovers (1409); Space vehicle instruments (1548)

1. Introduction

In recent years, interest in crewed lunar exploration has surged—not just for the Moon to be a stepping stone on the way to Mars, but also because of the many scientific investigations that would be made possible by the return of humans to the lunar surface (Crawford et al. 2012). The comprehensive and long-term human-tended activities envisioned by public and private organizations alike will pose severe logistical challenges if all supplies required to sustain these efforts must be brought from Earth. Local resources may therefore prove to be crucial for the establishment of a sustained human presence on the Moon: in situ resource utilization (ISRU), especially the extraction of water and oxygen, could substantially decrease the amount of material that must be resupplied to a lunar outpost (Meurisse & Carpenter 2020). Lunar water ice may very well be the single most important resource in (cis-lunar) space for decades to come—not just for the exploration of the Moon itself, but also for missions to other destinations in our solar system (Crawford 2015). Accessible deposits of water could, for example, be exploited to produce consumables of critical importance to both crewed and uncrewed missions, such as breathable air, potable water, and rocket propellant (Anand et al. 2012). They may even help to shield habitats and their inhabitants against cosmic and solar radiation (Singleterry 2013; Baiocco et al. 2018), another critical aspect of long-term missions beyond Earth orbit (Chancellor et al. 2018; Anderton et al. 2019). Any assessment of the possible uses of lunar water is, however, still severely constrained by the fact that we do not yet fully understand the extent and distribution of volatile deposits expected to exist at the lunar poles (Lucey et al. 2021; Landis et al. 2022). Even though several credible theories (solar wind, asteroid and meteorite impacts, and outgassing from the lunar interior) exist, we do not even know the exact origin of water (and other volatiles) on the Moon, because the currently

[13] Now at University of Central Florida, Orlando, FL, USA.

available data do not particularly favor any of the hypotheses put forward (Deutsch et al. 2020). While it is likely that all three mechanisms have contributed, or still contribute, to the delivery of volatile elements to the polar regions, further detailed and comprehensive (in situ) measurements will be required to fully understand the lunar water and volatiles cycle (Deutsch et al. 2020; Lucey et al. 2021).

In this paper, we present the results of a recently concluded concept and design study for a mission that is primarily intended to contribute to addressing the shortage of in situ data on volatiles, and in particular, water in the polar regions of the Moon. The study, called LUVMI-X, was funded by the European Union's Horizon 2020 research and innovation program; its primary objective was to raise the readiness of the technologies required to realize the mission to levels where a selection for full funding to develop a flight mission can be justified. We first summarize the scientific interest in the exploration of the Moon, with a focus on volatiles, mineralogy, and radiation, which are the key areas of interest for the mission's three main instruments. We then describe the mission's central element, a compact yet versatile rover, and the instrumentation it carries, before summarizing the measurements that can be performed. We present our strategy for identifying scientifically relevant candidate landing sites, and we present an example traverse on the Shackleton–Faustini range at the lunar south pole. To conclude, we discuss how the LUVMI-X mission fits into the diverse landscape of water- and volatile-focused missions currently under development in the US, Europe, and elsewhere.

2. The Science

By now, the existence of water ice in the Moon's polar regions is widely accepted, even though there is no consensus yet on the origin, extent, and nature of these deposits. The first indication for the presence of water ice at the lunar south pole was provided by the bistatic radar experiment aboard Clementine (Nozette et al. 1996), but was called into question by follow-up investigations (Stacy 1997; Simpson & Tyler 1999). In the years since, more evidence for lunar water has been gathered via neutron spectroscopy (Feldman et al. 1998; Mitrofanov et al. 2012) and via optical observations spanning the infrared, visual, and ultraviolet ranges (Clark 2009; Pieters et al. 2009; Sunshine et al. 2009; Hayne et al. 2015). The strongest evidence so far has been provided by LCROSS, which observed the ejecta plume of an impactor hurled into the permanently shadowed Cabeus crater and detected a water content of $5.6\% \pm 2.9\%$ by weight (Colaprete et al. 2010). While its origin is still not entirely clear (Deutsch et al. 2020; Lucey et al. 2020), water ice is thought to be trapped in regions of extremely low surface temperatures, primarily in large permanently shadowed regions (PSRs) and micro cold traps in the Moon's polar regions (Hayne et al. 2015; Li & Milliken 2017; Hayne et al. 2020). Yet recent results from the SOFIA airborne observatory suggest the presence of molecular water also in sunlit areas near the poles (Honniball et al. 2021), which may be caused by spillage of volatiles from the floor of PSRs onto the surrounding terrain due to micrometeoroid impacts and other processes (Farrell et al. 2015). Simulations confirm that surface ice should be stable on macroscopic scales in permanent cold traps inside PSRs, yet some recent calculations seem to suggest otherwise (Farrell et al. 2019). If buried under an insulating regolith layer of at least a few centimeters thickness, however, ice is almost certainly stable on geological timescales, perhaps even in areas covering as much as 15% of the lunar south pole (Paige et al. 2010). The impacts of micrometeorites over millions of years led to a breakup and mixing of surface-ice layers with the regolith beneath, in a process called *impact gardening* (Cannon & Britt 2020). Over time, this churning and overturning of material resulted in a heterogeneous and stable subsurface distribution of water ice and other volatiles up to depths of several meters (Costello et al. 2020). Models predict that the amount of water in these subsurface reservoirs is much larger than in the more easily accessible surface layers (Cannon et al. 2020).

The data available today, collected exclusively by remote-sensing instruments aboard probes in lunar orbit, constitute relatively strong but nonetheless preliminary evidence for the existence of water ice on the Moon. It is not yet clear whether potential reserves are vast and accessible enough to allow economically attractive extraction operations, either for commercial purposes or to ensure that crews of government-led exploration missions can depend on this water for their survival. Beyond water and other volatiles likely brought to the Moon by asteroids and meteorites (Prem et al. 2015)—or perhaps brought up from the lunar interior by volcanic activity (Wilcoski et al. 2022)—understanding the abundance and distribution of solar-wind implanted particles (SWIPs) is crucial for assessing their resource potential (Fegley & Swindle 1993). Besides these mostly practical aspects, lunar volatiles, and water in particular, may also help us understand the history of the inner solar system (Stoffler et al. 2006), the origin of water on Earth and other planets (Crider & Vondrak 2002; Svetsov & Shuvalov 2015; Barnes et al. 2016), and possibly even the delivery of prebiotic organic materials to the terrestrial planets (Chyba & Sagan 1992; Osinski et al. 2020). Aside from remote-sensing measurements, and with the notable exception of the samples recently collected by the Chang'E 5 mission, our knowledge about the concentration and distribution of water and other volatiles in the lunar rocks and regolith is limited to analyses of the few samples collected by the Apollo and Luna missions in the late 60s and early 70s of the last century. In situ measurements and sample-return missions, complemented by global high-resolution mapping from orbit, are required to resolve the ambiguities in current data and to identify suitable in situ resource utilization (ISRU) locations (Anand et al. 2012; Crawford 2015).

2.1. Mission Objectives

The mission's primary objective is to measure the concentration and distribution of volatiles in fully illuminated, partially illuminated, and permanently shadowed regions at the lunar poles. The principal target is water, both in the form of ice and in chemically bound states, but the abundances of other volatiles identified by LCROSS and found in Apollo samples—such as hydroxyl, hydrogen sulfide, ammonia, ethylene, and carbon dioxide (Colaprete et al. 2010)—shall also be determined. Measurements shall be taken through both remote sensing at standoff distances ($\sim$1 m) and direct sampling; the former having the advantage that it requires less time, while the latter can deliver higher levels of confidence. The combination of both techniques allows an efficient survey of volatile abundances over a relatively large area. To support

the investigation of the SWIP implantation and retention mechanisms, we aim to attempt the technically more challenging measurement of hydrogen and helium abundances with both techniques as well. An important secondary objective is the determination of the regolith's elemental composition in regions for which no reliable in situ or sample data exist yet, again with a focus on the polar regions. This shall be achieved through means of remote sensing, as an instrument for the in-depth mineralogical analysis of samples is beyond the envisioned scope of the LUVMI-X mission. Another secondary objective is the characterization of the lunar surface radiation environment in preparation for future crewed exploration missions. Here, we do not merely intend to measure the radiation dose astronauts will receive; we aim to conduct a full spectral analysis of charged and uncharged radiation from both primary and secondary sources.

3. Mission Elements

The scope of the concept and design study we present here was intentionally limited to the development of the surface element of the LUVMI-X mission. We did not devise a broader mission concept encompassing launch, transfer, and landing elements. Instead, we tried to make as few constraining design decisions as possible, in order to be able to take advantage of the growing landscape of commercial and government missions to the lunar surface, assuming that each of them will have identified appropriate means of getting to the Moon. The nature of the investigations we envision does, however, absolutely necessitate mobility—and thus the development of a suitable rover. Investigations using only lander-attached instrumentation were therefore excluded from our concept studies. Another constraint of the study was that any form of nuclear power source was prohibited, both in order to not constrain the choice of launch provider and due to lack of access to the required materials; the rover must therefore be powered by solar illumination only. This constraint significantly impacts the design of the surface element if it must survive the lunar night, during which temperatures drop well below 100 K in some regions (Williams et al. 2017, 2019). To limit the complexity and development time of the mission, we thus assumed a nominal operational period of 14 days during the lunar day, with only brief incursions into shadowed areas of no more than 8 hours. In principle, the rover and instrument designs presented here may, at specific landing sites and under certain conditions, be able to survive the lunar night—which at the poles can be as short as a few days—and could therefore allow much longer missions. Because we did not have the time to study night-time survivability in detail, and to reliably estimate the maximum time the rover could operate in shadow, we have settled on conservative assumptions for these capabilities and will leave detailed investigations to future studies.

3.1. The Rover

LUVMI-X's surface element is a compact four-wheeled rover (see Figure 1) capable of traversing a distance of at least 5 km during a 14-day mission. The rover is optimized for operations in the lunar polar regions and is well suited for short-term investigations of PSRs and other cold traps. It is equipped with four independently steerable wheels in a rocker configuration with an internal differential, has a ground clearance of 30 cm, and drives at a nominal speed of up to $10\,\mathrm{cm\,s^{-1}}$. We chose a four-wheeled design because it allows substantial mass savings over a six-wheeled configuration, but if combined with a rocker mechanism, it has only marginally worse stability and traction. Though the design offers less redundancy than one with six wheels, we consider this to be an acceptable drawback given the short mission duration and our goal of designing an affordable platform. The wheels consist of two lightweight aluminum rims connected to a hub via spokes; the running surface is made of wire mesh, to prevent the rover from sinking into loose soil, and is equipped with grousers for increased traction. To achieve high drive torque, we embedded frameless and brushless motors with harmonic gears directly into the wheels' hubs. One of the distinguishing features of the vehicle is its actuated suspension, which allows bringing chassis-mounted instruments into contact with the lunar surface. It also allows modifying the rover's center of mass, and hence stability, to adapt to different terrain conditions. The vehicle is designed to traverse obstacles up to 40 cm in height and climb slopes composed of loose material with inclinations of up to 25°. Figure 2 shows a prototype rover whose drive train and wheel design closely resemble those of the flight version. Using the prototype, we were able to demonstrate most of the rover's mobility capabilities. The surface composition at the test site did not, however, allow us to fully verify the rover's ability to climb slopes of material that is representative of lunar regolith. Power is generated by a vertically mounted, rotatable solar panel conceived to work best at high latitudes; our models indicate that the panel should be capable of delivering up to 150 W. About half of the generated power is available for the scientific instrumentation. The thermal control system is likewise optimized for low illumination angles, and hence it features upward-facing radiators. Nominally, the rover will communicate via an *X*-band direct-to-Earth link, though relaying signals through a lander or satellite is possible and preferred, should these options be available.

The mission is nominally teleoperated, mainly relying on a suite of cameras for visual feedback; we do, however, plan to have the option of performing a limited set of supervised, semi-autonomous operations should environmental conditions or operational constraints require it. To aid both operational modes, the rover is equipped with hazard-detection and navigation cameras; the former are mounted on its forward- and backward-facing surfaces, while the latter are mounted on a pan/tilt unit on top of the antenna mast. The navigation cameras are based on commercially available, space-grade camera modules. They provide three-dimensional images with multispectral resolution for short focus distances (0.1–1 m) and regular three-dimensional images for medium distances (1–10 m). They also include a long-range telescope for traverse planning and for identifying potential sites for investigation with the rover's scientific instruments. The pan/tilt mechanism and the distance information encoded in the three-dimensional images also allow the acquisition of panoramic digital elevation models (DEMs) to support rover navigation. As an alternative to this relatively traditional setup, we developed a technology demonstrator of a 360° stereo camera. The system is integrated into the antenna mast—avoiding the need for the mass and complexity of a pan/tilt mechanism—and would allow a more efficient use of mission time, as only a single exposure is required to image the surroundings of the rover. The camera's stereo capability also allows for the creation of DEMs of the entire local area visible to the rover, and for calibrated distance

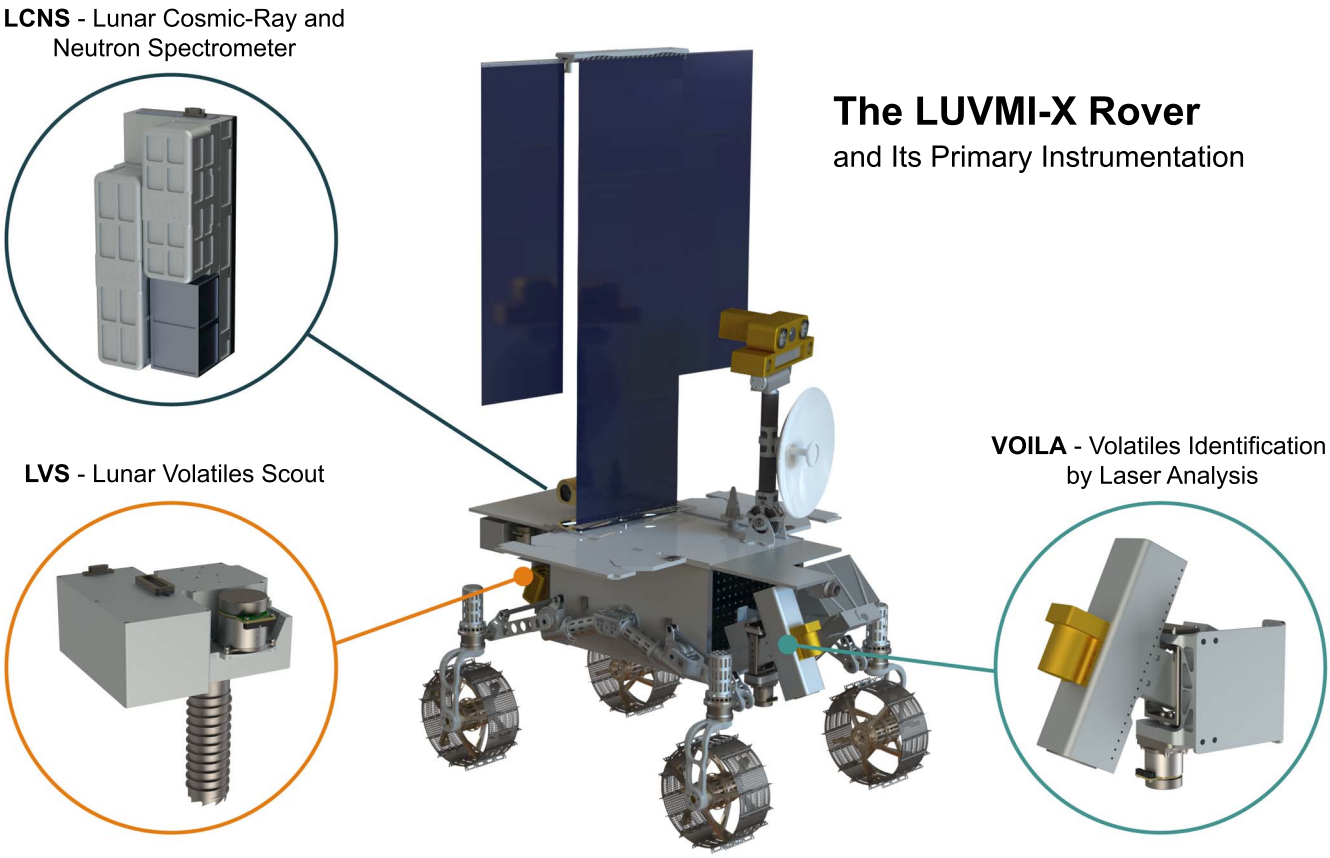

Figure 1. The LUVMI-X rover and its instrumentation.

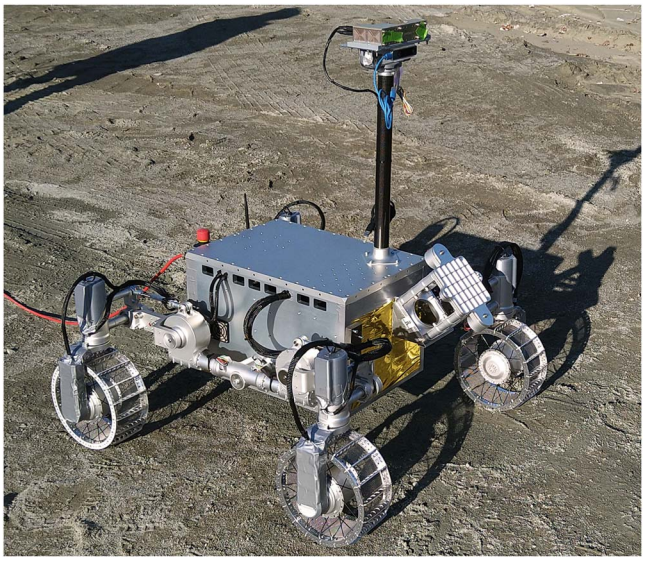

Figure 2. Rover prototype during field testing.

measurements of specific features. Such a 360° camera system could vastly reduce the number of cameras required on the rover—and thereby reduce the mass, required power, and complexity of the mission.

The rover can accommodate instruments (payloads) with a total mass of 25 kg, distributed mainly on the forward- and backward-facing surfaces of its chassis. A limited volume inside the chassis is available for payload systems that need to operate in a more tightly controlled thermal environment than achievable on the outside (within the volumetric, mass, and power constraints). This payload capacity matches the one required for the instruments of the LUVMI-X concept mission described in this paper, but would also allow the rover to carry a wider variety of payloads in future missions, due to its modular design. Instruments can either be mounted directly to the rover chassis or can be deployed to the lunar surface using custom release mechanisms (and the rover's actuated suspension). This allows us to place instruments in areas of interest for long-term investigations while the rover continues its journey. The mechanism also allows the retrieval of payloads after they have completed their investigation. Such instruments would be self-sufficient, rely on battery or solar power, and use low-power radio links to stay in contact with the rover or to communicate directly with orbital relay satellites. We also devised a spring-loaded mechanism that can deploy instruments with masses up to 1 kg into areas that are inaccessible to the rover, such as deep craters, at distances of up to 50 m (in lunar gravity). This capability allows us to investigate extremely hazardous areas that would otherwise be unreachable but may hold large PSRs or other scientifically interesting features.

3.2. Scientific Instruments and Objectives

We selected the rover's scientific instruments such that they provide complementary data on the mission's primary target: water. We are currently developing three major instruments that can search for water and other volatiles on the surface and at different depths.

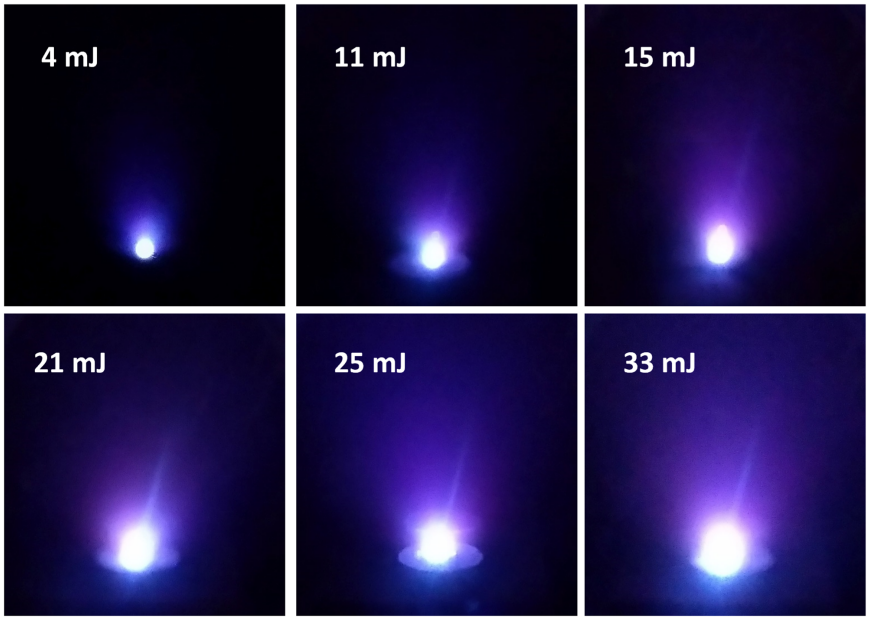

Figure 3. Plasma plumes generated by pulses of different energies on regolith simulant.

Starting on the surface, the Volatiles Identification by Laser Analysis (VOILA) instrument will be able to detect the signatures of hydrogen and oxygen in the upper few millimeters of the regolith, allowing us to determine the amount of surface ice present in the areas we investigate. VOILA uses laser-induced breakdown spectroscopy (LIBS) to rapidly analyze the composition of samples along the rover's path. LIBS relies on ablating material from a sample by focusing a pulsed laser onto its surface, producing a microplasma of atoms, ions, and electrons (De Giacomo & Hermann 2017) in a plume several millimeters in size. We developed a compact Yb:YAG laser emitting at a wavelength of 1030 nm that can generate pulses at a rate of 10 Hz, each with a length of 8 ns and an energy of more than 15 mJ. Laboratory measurements have shown that this energy is large enough to produce a sufficiently bright plasma even in loosely grained regolith simulant at near-vacuum pressures (Richter et al. 2021). As an example, Figure 3 shows plasma plumes generated by laser pulses of different energies. The light emitted by the plasma is collected by the instrument's optical head with an aperture of 50 mm, and its spectrum is analyzed to identify and quantify elements based on their characteristic emission lines. We use a crossed Czerny–Turner spectrometer that provides spectral coverage from 350 to 790 nm at a resolution of better than 0.5 nm and that is optimized for the detection of hydrogen at 656.3 nm and of oxygen at 777.4 nm. To save mass and reduce the complexity of the system, the same confocal optics are used to collect the plasma light and to focus the laser onto its target. The focusing mechanism produces a laser spot size of less than 190 μm and guarantees repeatable measurement conditions on the uneven lunar surface at distances between 0.3 and 0.5 m; a pointing mechanism allows to analyze targets within a lateral field of view of about 40° in front of the rover. The light of an LED operating in the visible spectrum can be coupled into the receiving path of the optical system and be focused on the target the instrument is observing. The resulting visible spot of light can be detected by the rover's forward-facing hazard-detection cameras and be used to calculate the distance to the target. A dedicated camera is mounted to the instrument for monitoring the target before and after sampling, providing information on the ablation pattern to aid the analysis of measurements. Our laboratory measurements with prototypes and simulants mixed from basalt and gypsum indicate that water concentrations of at least 1.0% by weight are clearly detectable with the VOILA instrument. We are performing further studies to demonstrate even lower detection of 0.5% by weight or better. Besides gathering data on surface ice, the instrument will also be able to detect and quantify all major rock-forming elements—i.e., magnesium, titanium, aluminum, silicon, calcium, sodium, and potassium—and can thus determine the composition of regolith and rocks for a more comprehensive geochemical analysis of the mineralogical composition of the lunar surface. Laboratory tests are still ongoing, but early measurements showed that relevant minerals can be clearly distinguished from each other.

To investigate the shallow subsurface, the Lunar Volatiles Scout (LVS) will be able to sample the lunar soil to depths of about 15 cm and gather data on the changing volatile content with depth (Biswas et al. 2020). It consists of a combined sample drill and volatile-extraction oven that can be inserted into the regolith to release volatiles, and of a miniature ion-trap mass spectrometer (ITMS) for the elemental analysis of the released gases. The sampler consists of a hollow auger drill shell that encloses a sample volume. A resistive heater located at the center of the sample volume can heat the surrounding regolith to a maximum temperature of about 750°C, depending on the abundance of volatiles in the enclosed sample (a higher abundance leads to a higher thermal conductivity and hence to a lower temperature). Such temperatures allow to release loosely bound (physisorbed) volatiles like water (Poston et al. 2013; Kleinhenz et al. 2018) and are likely also sufficient for releasing chemically bound ones (Hibbitts et al. 2011). Based on laboratory tests with JSC-1A simulant, we foresee a baseline heating duration of 90 minutes at a constant power of 15 W, which will allow us to reach 750°C while avoiding sintering at the heating rod. Shorter sampling durations would, for example, be used inside a PSR, where the focus of investigations lies on physisorbed volatiles and lower

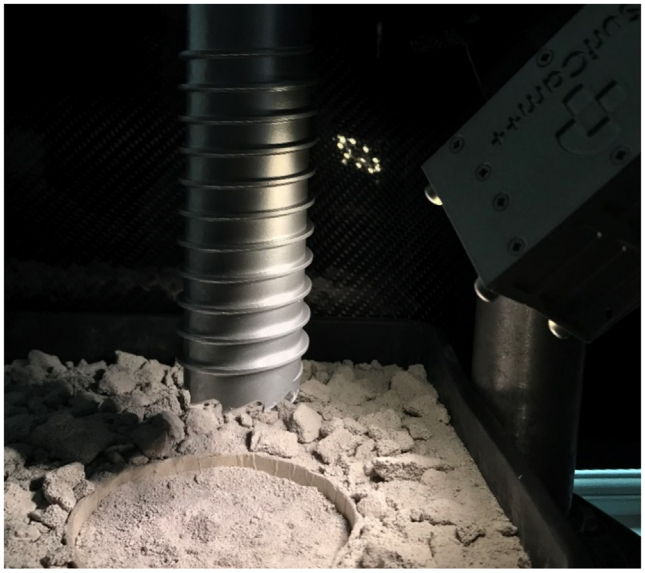

Figure 4. Drill prototype illuminated by the LVS-dedicated multispectral camera during testing.

temperatures are therefore sufficient. Taking the additional time required for drilling, extraction, and imaging of the sample site into account, the nominal duration for a sampling operation is about two hours. Pirani sensors measure the gas pressure inside the sample volume, to provide some initial indication of the abundance of volatiles. The released gases are detected and characterized by the miniature ITMS, whose design we derived from the Ptolemy instrument that provided the first in situ measurements of volatiles on the surface of the comet 67P/Churyumov–Gerasimenko during the Rosetta mission (Morse et al. 2012; Wright et al. 2015). The ITMS is mounted directly on top of the drill and is connected to the sample volume via a small orifice for pressure control. Even though it is a mechanically simple device, it is capable of detecting a wide range of ion species (with mass-to-charge ratios, m/z, of 10–200) with a parts-per-million sensitivity across the detection range. This sensitivity allows the LVS to detect all volatiles species that have previously been detected in the LCROSS ejecta plume, though we were not yet able to determine whether individual compounds could be unambiguously identified if they are all present in the same sample. However, because of the inherent sensitivity limitations of an ITMS at low masses, it will be challenging to determine the relative concentrations of smaller molecules such as water, hydroxyl, and ammonia, due to their similar fragmentation patterns (Biswas et al. 2020). We are studying the feasibility of using a miniature magnetic-sector mass spectrometer to measure hydrogen and its isotopes, and have developed a prototype as part of the concept study presented here. A dedicated camera provides multispectral three-dimensional images and videos of the drilling operations, allowing us to assess the geotechnical properties of the regolith at the sampling site. It can also monitor the tracks left by the rover's wheels to aid operations. Figure 4 shows a drill prototype being illuminated by the camera during testing. In its prototype configuration, the system is sensitive to the wavelengths of 450 nm, 540 nm, 600 nm, 660 nm, 725 nm, 840 nm, 940 nm, and 970 nm, which lie in the typical range for lunar-exploration instruments (Robinson et al. 2010; Green et al. 2011). With the LVS data, we will be able to provide new insights into the vertical distribution of water ice and other volatiles in the surface layer, and it will help improve our understanding of the mixing processes resulting from impact gardening.

The third major instrument we conceptualized for the LUMVI-X mission is the Lunar Cosmic-Ray and Neutron Spectrometer (LCNS), which will measure the abundance of hydrogen in the soil beneath the rover, down to depths of about a meter, and characterize the radiation environment on the lunar surface (Losekamm et al. 2022). The LCNS consists of several sensors, each specialized for the measurement of different aspects of the charged and uncharged radiation field. Using the instrument's compact neutron spectrometer (CNS), we will search for water and hydroxyl deposits by measuring the (relative) fluxes of thermal, epithermal, and fast neutrons. These are created by highly energetic cosmic rays that penetrate the lunar surface to depths of several meters. While a fraction of the produced neutrons diffuse upward through the regolith, they scatter with the soil's constituent nuclei and assume an energy spectrum that is characteristic for the composition of the regolith (Peplowski et al. 2016). The presence of hydrogen (and thus water or hydroxyl) elicits a detectable change in this energy spectrum by lowering the relative flux of epithermal neutrons. The CNS is based on an adaptation of the Bonner sphere (Bramblett et al. 1960) and is a conceptually simple yet robust and quite capable instrument. We implemented a linear detector geometry, using solid-state thermal-neutron detectors (cerium-activated scintillators), active moderators, and highly efficient neutron absorbers. This linear geometry allows us not only to detect epithermal and fast neutrons after they have been moderated to thermal energies but also to measure their energy loss in the moderation process, thus allowing us to determine their total energy. Extensive performance simulations have shown that the CNS can identify detected thermal neutrons (those with energies from 0.1 to 0.4 eV) with an accuracy of 98%; if the detection efficiency is taken into account, almost 90% of the incident thermal neutrons are correctly measured. In the epithermal range (0.4 eV to 0.6 MeV), the classification is marginally better, but the combined efficiency drops to approximately 46% due to the much lower interaction cross section (interaction probability) for neutrons of these energies. For fast neutrons (0.6–8 MeV), the classification decreases to about 46% at a slightly higher combined efficiency of 49%. Overall, these performance parameters should be sufficient for collecting statistically meaningful data even during rover traverses. If combined with data from the LVS, the measurements of the CNS will allow us to help refine our understanding of the vertical distribution of water in the lunar soil. To measure cosmic and solar radiation, the instrument's charged-particle telescope (CPT) must be sensitive to radiation particles with a wide range of charge, mass, and energy. Again, we opted for an integrated, linear design: a telescope comprising three flight-proven silicon pixel detectors (Granja et al. 2016) encloses a calorimeter made from plastic scintillators and absorbers with high atomic mass. Two silicon detectors on top of the calorimeter stack provide directional information for low-energy particles; the third detector below the stack provides a longer lever arm for particles traversing the full detector. The calorimeter not only measures the energy a particle loses in the detector—or its total energy if it stops inside the stack—but also allows to identify its species using a method called Bragg curve spectroscopy (Gruhn et al. 1982). We can thus measure particle-dependent

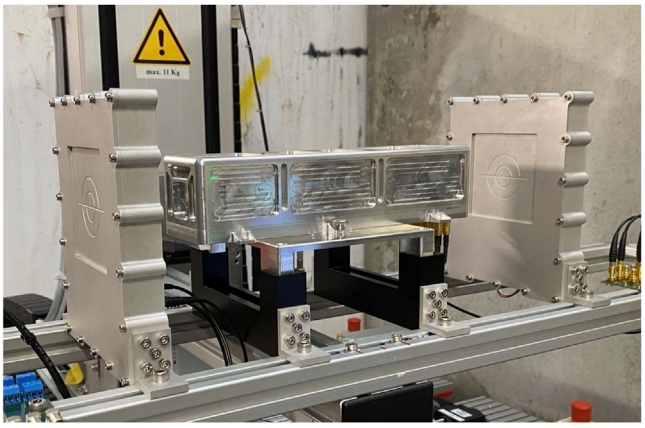

Figure 5. Functional testing of the LCNS charged-particle telescope with a proton beam.

spectra for protons with energies larger than 10 MeV and ions with energies larger than 50 MeV per nucleon. Figure 5 shows a prototype of the CPT during functional testing with a proton beam. Because the lunar proton albedo may also contain information about the distribution of volatiles in the regolith (Schwadron et al. 2016), we included a small telescope consisting of planar silicon detectors that is sensitive to protons and electrons with energies of less than 1 MeV scattering off the lunar surface. The CPT's measurement capabilities, combined with those of the CNS and several additional dosimeters, allow us to fully characterize the radiation environment on the lunar surface—including the dose contributed by neutrons—which is a crucial prerequisite for future crewed exploration missions (Reitz et al. 2012). Its data are also crucial for the analysis of CNS measurements, which requires knowledge of the intensity of cosmic and solar radiation for normalization.

These three primary instruments are complemented by the Volatiles and Context Analysis Suite (VCAS), a self-sufficient instrument suite that can measure volatiles in locations that are too difficult or hostile for a rover to access—for example, on steep slopes or inside deep craters and lava tubes. At the core of the VCAS is a miniaturized magnetic-sector mass spectrometer optimized to fit into a form factor that fits inside the rover's spring-loaded deployment mechanism. It will allow us to detect molecular water and other volatiles outgassing from the regolith—for example, in locations with changing illumination conditions. The instrument will also provide supplementary information about the site it has been deployed to, including images of the local geology, rock formations, and illumination, as well as measurements of the physical, mechanical, and thermal properties of the regolith. Several additional sensors can measure the local temperature and dust distribution to study the near-surface exospheric particulate environment. VCAS units will be released from the rover using the deployment mechanisms described above, depending on the accessibility of the area that shall be investigated.

4. Concept of Operations

As the launch, transfer, and landing elements for the LUVMI-X mission were not part of the study presented here, we focus our discussion of the operational concept on the time after landing. Due to the rover's low mass of about 75 kg (including instrumentation) and its compact stowage configuration, we can hitch a ride on many of the lunar landers currently under development—including Astrobotic's Peregrine and Lockheed Martin's McCandless landers, which we used as representative references during the study. Given that these or other (commercial) landers with comparable capabilities will be available very soon, we expect at least one, if not several, missions to target the lunar south pole. Nonetheless, even though our main scientific interest lies in investigating volatiles in the Moon's polar regions, the rover and its instruments are also compatible with nonpolar landing sites in case a suitable flight opportunity presents itself before a polar opportunity arises. The scientific return of such a nonpolar mission would, however, most likely not be as comprehensive as the scenario we aim for and present here. Because the rover's night-time survival capabilities are limited, we assume a maximum mission duration of 14 days at latitudes of 75° or higher, during which the mission will need to operate under almost continuous illumination. Excursions into partially illuminated and permanently shadowed regions are possible, however, and can last about six hours at a time, with significantly more time required to recharge batteries between consecutive excursions. We design all systems to survive short lunar nights of up to 24 hr in hibernation mode.

Figure 6 provides a visual guide for the discussion of the mission's concept of operations. After a successful deployment to the lunar surface, we will first use the LVS and VOILA instruments to perform a detailed investigation of the landing site. The primary objective of this early phase of the mission is to assess the degree to which the surrounding area was disturbed and altered by the lander. A thorough understanding of the nature and extent of the contamination and alteration of the lunar surface resulting from the action of the lander's engines during descent will be of great importance to follow-on missions, in particular those without a mobile element. In these missions—where it is unlikely that the lander's instruments will be able to access uncontaminated regolith, even if using a robotic arm—knowledge of the distribution of contamination and how it varies with distance from the lander, as well as empirical data on how the exospheric abundance of volatiles freed or generated by the lander's motors evolves with time, will be crucial for a correct interpretation of measurements. If a suitable rock or boulder is located close to the lander, we also plan to assess how much shielding from the descent motor's exhaust plume it provides. During this early phase, the LVS will mostly operate in what we call *sniffing mode*, in which the instrument's mass spectrometer measures exospheric volatiles freed from the regolith by mechanical and thermal perturbations caused by the lander and rover. Using VOILA, we will be able to assess the degree to which volatiles of the lander's exhaust were implanted into the top layer of the regolith by performing measurements at increasing distance from the landing site. To determine how deeply volatiles were implanted, we will also use the LVS to sample the subsurface volatile abundance at different depths in select locations.

To further our understanding of the processes leading to the accumulation of surface ice, we will first direct the rover to an undisturbed site at which a boulder or some other rise in the terrain creates an area of temporary shadow. Orbital observations revealed a global cycle of hydration and dehydration due to diurnal illumination (and hence temperature) changes (Clark 2009), which likely drives the migration of volatiles toward permanent cold traps at the poles (Crider & Vondrak 2002). In the polar regions, even

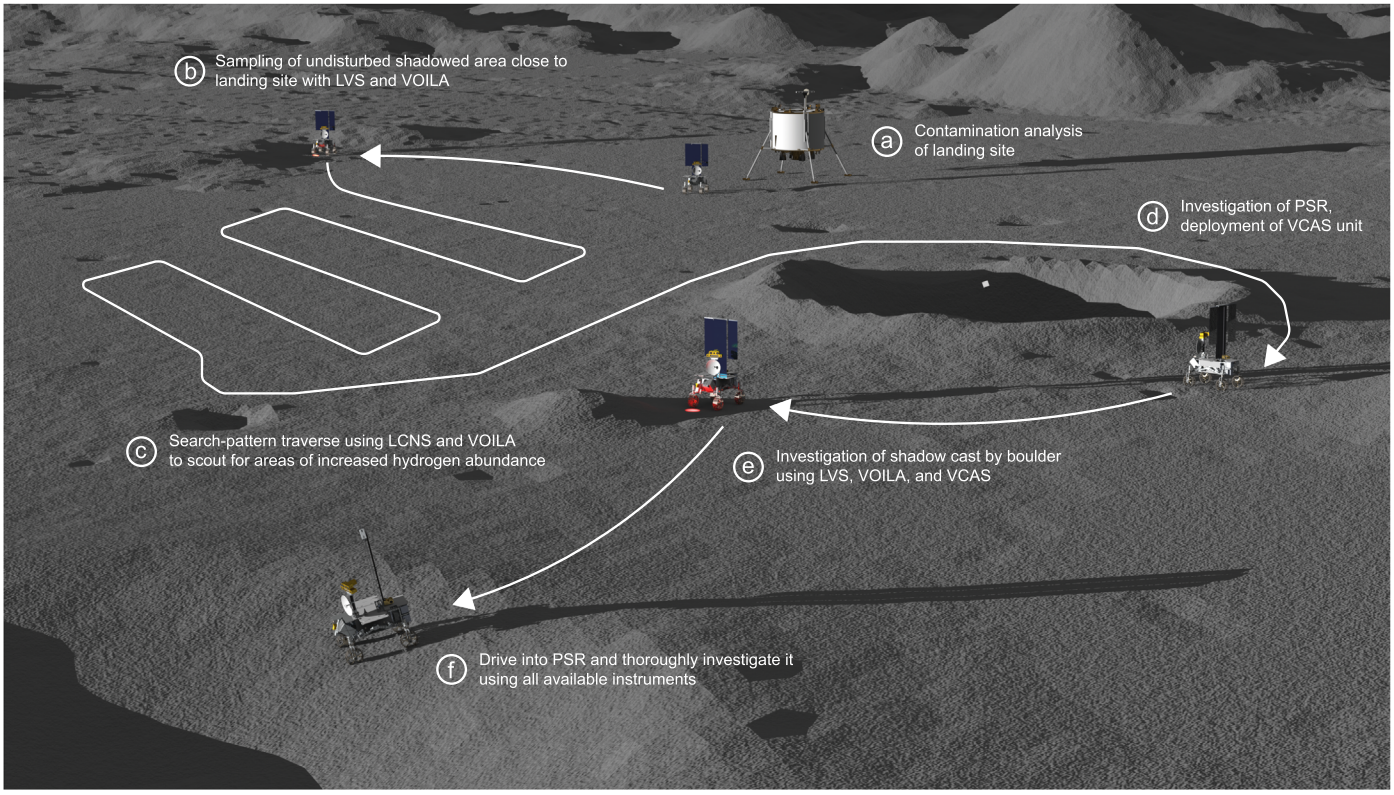

Figure 6. Visual guide (not to scale) to the mission's concept of operations: contamination analysis of the landing site (a), sampling with the LVS and VOILA (b), scouting for increased hydrogen abundance during traverse (c), investigation of PSR and deployment of a VCAS unit (d), sampling of an area in temporary shadow with VOILA and LVS (e), and drive into PSR (f).

small boulders can cast large and long-lasting shadows due to the Sun's low elevation and the Moon's long diurnal cycle of 29 days. The regolith in these shadowed areas can cool down significantly enough for volatiles to freeze onto its surface, while the illuminated side of the boulder will become very hot. Sampling the soil on both sides of a suitable boulder with the LVS and VOILA instruments will provide new insights into the diurnal hydration cycle and may help us understand how water ice and other volatiles accumulate in transient cold traps. If the timing is right, further data could be provided by a VCAS unit placed into a shadowed area shortly before the night–day terminator moves over it. The sudden increase in temperature after sunrise would free volatiles from the regolith, leading to an increased exospheric abundance that could be detected by the mass spectrometer in the unit. A retrieval of the instrument would allow to repeat and compare measurements in locations with different illumination (and hence temperature) conditions.

After these initial investigations that can be performed directly at or close to the landing site, we will instruct the rover to begin its traverse toward nearby volatile-rich locations (e.g., cold traps inside PSRs). The LCNS, which will be switched on upon landing and continuously operate from then on, will allow the identification of areas with increased hydrogen abundance during the traverse. Upon detection of such areas, or at regular intervals otherwise, the VOILA instrument will probe the top layer of the regolith in order to confirm whether a surface-ice layer—or more generally, an increased hydrogen abundance—is present. Depending on the significance of the hydrogen signature found by the LCNS and VOILA instruments, the rover will stop its traverse, perform an extended set of measurements with VOILA, and subsequently sample the regolith at different depths with the LVS. The time required for these operations will also allow the LCNS to gather a more statistically significant data set on the local hydrogen abundance. During the traverse, we will use the rover's navigation cameras to record DEMs and panoramic images of the lunar surface in order to identify sites of interest for the mineralogical analysis of rocks or regolith with the VOILA instrument. Potential micro cold traps identified in the images will be investigated using the VOILA and LVS instruments. Depending on the topography of the surface along the traverse path, the exospheric abundance of volatiles after terminator passages could be characterized with deployable VCAS units or using the LVS in sniffing mode—with the latter option likely providing a higher measurement resolution—in multiple locations, to collect additional data on the migration of volatiles.

Once the rover arrives at a sufficiently large PSR holding a permanent cold trap, we will use its three main instruments to perform a survey of volatile abundances in the surrounding area as a function of distance from the PSR rim. Not only does this provide a reference for measurements inside the PSR, it also allows us to investigate the spillage of volatiles from the PSR caused by micrometeoroid impacts. We will then use the rover's spring-loaded mechanism to propel a VCAS unit into the PSR. Equipped only with a mass spectrometer for the measurement of exospheric volatile abundances, the unit will not be able to actively sample the soil. Instead, we must rely on the instrument's waste heat and the physical disturbance caused by its tumble into the PSR to free physisorbed volatiles in the

uppermost layer of the regolith, which can then be detected by the mass spectrometer. Environmental conditions and operational constraints permitting, the rover shall investigate at least one additional PSR in the same manner. Finally, once we have identified a sufficiently shallow and accessible PSR with a permanent cold trap inside, we will direct the rover to drive into it after the survey of the surroundings is completed. Using all available instruments, we will perform a thorough investigation of the surface and subsurface volatile abundances. We may even discover a solid layer of water ice on the surface or buried by just a few centimeters of regolith. This final and most risky investigation is the nominal end of the LUVMI-X mission. Should the rover make it out of the PSR, additional investigations may be conducted until the onset of the lunar night.

5. Candidate Landing Sites and Traverses

To understand how the rover's capabilities drive, or perhaps constrain, the scientific potential of the mission, we performed an analysis of possible landing sites and rover traverses. For simplicity, we focused on the abundance of water (and other volatiles) as the primary criterion for selecting a target area. Even though there may be great scientific interest in performing geological analyses and radiation measurements virtually anywhere on the Moon, we concluded that, for practical purposes, there is a high priority for performing them in areas with high potential for water deposits. We limited our work to the lunar south pole, within a latitude range from 75°S to 90°S, because of its larger total PSR surface area compared to the north pole and the corresponding higher probability of finding suitable landing sites with surface-ice deposits. The south pole is also the target of many upcoming missions that may provide ride-share opportunities to LUVMI-X. We first performed a regional analysis using multiple criteria to identify regions of interest (ROIs) based on our scientific objectives and on the capabilities and constraints of the rover and potentials landers. We then performed a high-resolution local analysis of these ROIs to identify possible landing sites and rover traverses that fulfill the scientific objectives of the LUVMI-X mission and are in line with the concept of operations described above. As launch, transfer, and landing elements were not part of the study presented here, we again used Peregrine and McCandless as representative examples of (commercial) lunar landers currently under development.

5.1. Data and Methods

For the work reported here, we only used peer-reviewed and publicly released sets of data; most of them are available through NASA's Planetary Data System (PDS). Those that are not can be downloaded from the instruments' websites. For the regional analysis, we used data sets with global coverage and varying resolution:

1. the most recent version of the Lunar Reconnaissance Orbiter's (LRO) LROC Wide Angle Camera mosaic at 100 m px^{-1} (Speyerer et al. 2011);
2. several digital elevation models based on data from the Lunar Reconnaissance Orbiter (LRO)'s laser altimeter (LOLA) at resolutions between 10 and 120 m px^{-1} (Smith et al. 2017);
3. the hydrogen abundance from Lunar Prospector NS data at 15 km px^{-1} (Elphic et al. 2007);
4. the hydrogen abundance from LRO LEND data at 2 km px^{-1} (Boynton 2009; Mitrofanov et al. 2012);
5. the average visibility of the Sun and Earth and a map of PSRs at 240 m px^{-1}, derived from LRO LOLA data (Mazarico et al. 2011; Gläser et al. 2018; Barker et al. 2021);
6. and a predictive model of ice stability at depth at 200 m px^{-1} based on LRO Diviner data (Paige et al. 2010).

For the local analysis, we used:

1. the LRO's Narrow Angle Camera mosaic at an average resolution of 1 m px^{-1} (Wagner et al. 2015);
2. the digital elevation model derived from LOLA data, but with a resolution of 5 m px^{-1} for the highest latitudes (Smith et al. 2017);
3. evidence for surface ice from the Moon Mineralogy Mapper (Li et al. 2018);
4. illumination maps based on LRO data at 60 m px^{-1} (Speyerer & Robinson 2013; Gläser et al. 2018);
5. the average visibility of the Sun and Earth and a map of PSRs from LOLA data, but with a higher resolution of 60 m px^{-1} (Mazarico et al. 2011; Gläser et al. 2018; Barker et al. 2021);
6. and the same model for ice stability at depth we used for the regional analysis.

We processed the data with the ArcGIS software, using a polar stereographic projection with a latitude range from 75°S to 90° S centered at the south pole.

To define and then select ROIs, we first applied a number of constraints: (a) To ensure a safe landing, slopes in the region must be less than 10° in an area large enough to hold the landing ellipses of Peregrine (24×6 km) or McCandless (2×2 km); (b) at least one PSR must be in close proximity to the landing site, at a distance of no more than 5 km; and (c) the abundance of hydrogen in the general area must be in excess of 100 ppm. We used these constraints to find areas that would generally be suitable for landing a mission. In parallel, we calculated the scientific potential of sites based on a weighted-sum scoring system using four criteria with different weights: the visibility of the Sun (higher is better; weight of 0.5), the depth at which water ice is expected to be stable (shallower is better; weight of 0.25), the visibility of Earth (higher is better; weight of 0.15), and the hydrogen abundance in excess of 100 ppm (higher is better; weight of 0.1). We assumed the mission to take place in December and January, during the time of higher illumination at the south pole (Bussey et al. 2010), to adjust for seasonal variations in solar illumination. To account for the fact that sites with high scores of scientific potential may not necessarily lie in areas that are suitable for landing, we then identified lander-compatible areas within 5 km of top-scoring sites.

In our local analysis using high-resolution data sets, we placed potential landing ellipses inside the most suitable ROI and ranked them by a weighted sum of Earth and Sun visibilities. For each ellipse and its surrounding 5 km area, we identified candidates for the four major waypoints that must lie along the rover's path: (a) a shadowed boulder to place a VCAS unit at; (b) a subsurface cold trap to investigate with the LVS; (c) a cold trap inside a PSR inaccessible to the rover to deploy a VCAS unit into using the spring-loaded deployer; and (d) a PSR holding a permanent cold trap that the rover can

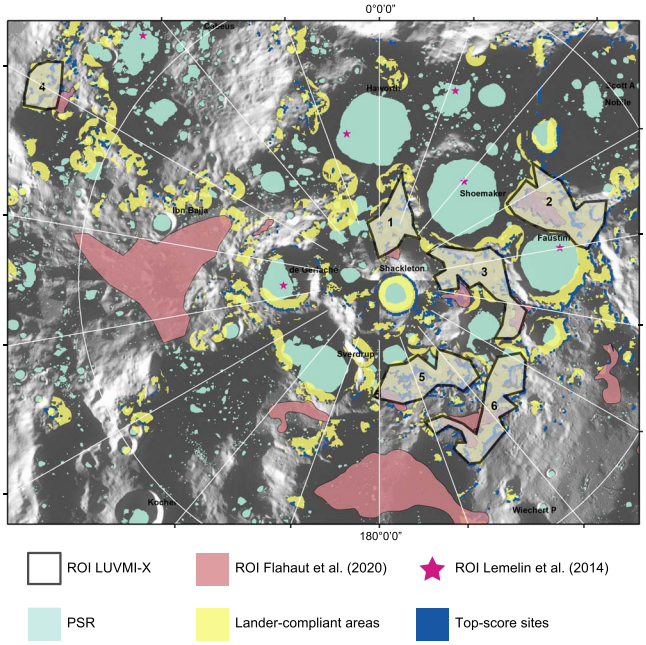

Figure 7. Regions of interest for the LUVMI-X mission, compared to those previously identified by Lemelin et al. (2014) and Flahaut et al. (2020).

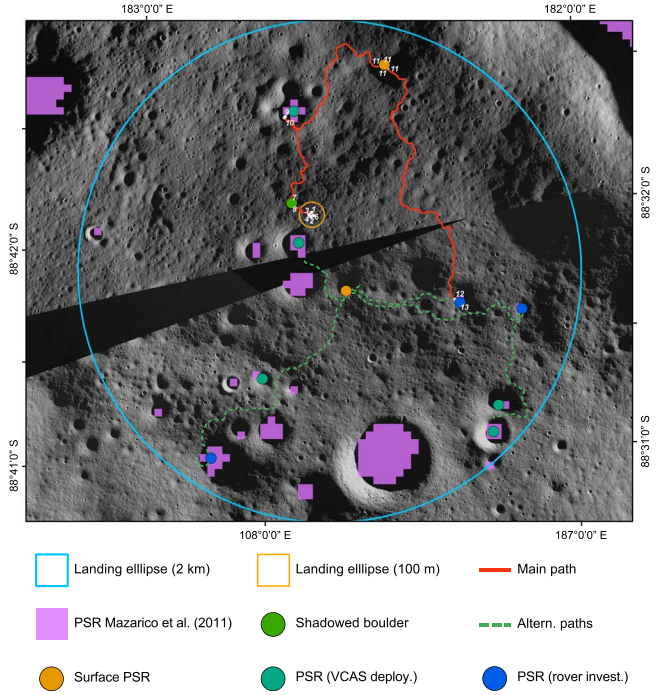

Figure 8. A possible traverse path (red line) on the Shoemaker–Faustini ridge fulfilling all requirements for the mission. Alternate paths for landings outside of the 100 m landing ellipse are shown as dashed green lines.

drive into and investigate. We strongly favored regions in which subsurface ice is stable at less than 20 cm depth, to allow sampling with the LVS. To select waypoints and construct a traverse path between them, we also took into account two major constraints imposed by the rover: a maximum slope of 20° and a maximum traverse length of 150 m inside a PSR. The latter constraint is caused by the rover's limited ability to survive without sunlight, and assumes that it will move at an average of one meter per minute while in shadow. Extended science operations may further reduce the distance it can drive inside the PSR. As the rover will mostly be teleoperated, we favored waypoints and traverses with high Earth visibility.

5.2. Results

Figure 7 shows the six ROIs we identified, which mostly lie in the vicinity of the Shackleton, Shoemaker, and Faustini craters. The figure also shows the ROIs previously identified by Lemelin et al. (2014) and Flahaut et al. (2020). It is evident that our ROIs have little overlap with them, though this can be explained by the different constraints that were applied. Lemelin et al. concentrated on regions inside PSRs, which we excluded because the LUVMI-X rover is solar-powered. Flahaut et al., on the other hand, concentrated on areas with exposed surface ice, so their ROIs only partially intersect with ours. All six ROIs comfortably fit the McCandless landing ellipse of 2×2 km, but none of them truly fit the one for the Peregrine lander (24×6 km). We therefore limited our subsequent analysis to finding suitable sites for the smaller of the two landing ellipses. We also assumed that the lander is capable of targeting a 100×100 m area inside the ellipse once it is close enough to rely on its own optical sensors, based on documentation available from Lockheed Martin (Lockheed Martin Corporation 2019). We identified ROIs #2 and #3 as the most promising candidates because of their high abundance of hydrogen and low surface temperatures. We ultimately concluded that ROI #3, located on the Shoemaker–Faustini ridge, has a higher potential of capturing and retaining volatiles, and should therefore be the primary target of the LUVMI-X mission.

We identified five possible landing ellipses inside ROI #3 and ranked them, again using a weighted sum of Sun visibility, Earth visibility, and topography. As an example, Figure 8 shows a landing ellipse and possible traverse path of 5.6 km length that fulfill all waypoint requirements. It is not optimized for power consumption, however, and it also features a relatively large PSR close to the landing site. Besides the primary traverse, the figure also shows optional paths the rover could take depending on the exact landing site and available power. We identified several other possible traverses that fulfill the mission's requirements and constraints to varying degrees.

The analyses we present here have obvious limitations and may only be considered preliminary. The digital elevation model we used does not reflect features under 5 m in size. Even though this can be partially mitigated by relying on the higher-resolution optical images, it still limits our ability to plot a safe traverse for the rover. In addition, some areas in the ROIs we identified were in shadow at the time they were photographed by the LRO cameras, giving us no option to manually identify possible obstacles in these regions either. Earth and Sun visibilities were only available at a resolution of 60 m and are averaged over a period of 18.6 yr (Mazarico et al. 2011), leading to significant uncertainties in the actual visibilities of the Sun and Earth at the time of the mission. The predicted ice-stability and temperature maps have even lower resolutions of 200 m and 240 m, respectively. We also had to make assumptions about the landers' imaging capabilities and landing accuracy. In our analyses, we did not treat the uncertainties resulting from these limitations and assumptions at all. The results must therefore be understood as a general proof of feasibility of the LUVMI-X mission concept: We were able to demonstrate that—given the constraints imposed by the rover and commercial landers currently under development—

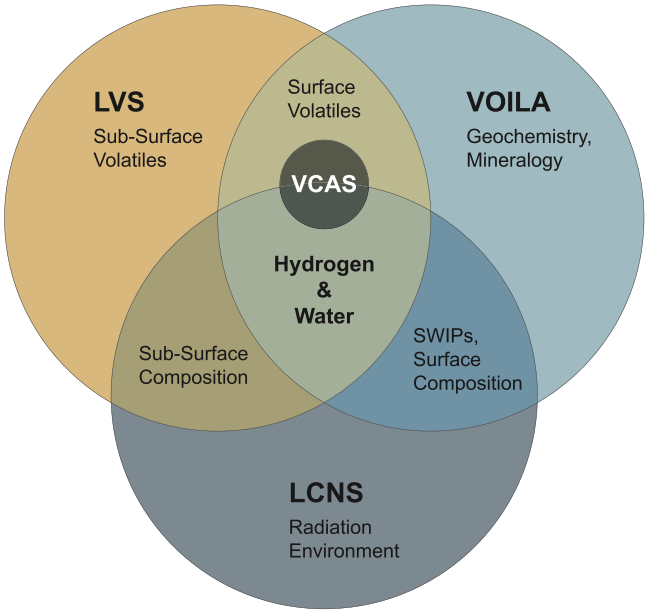

Figure 9. LUVMI-X instruments and scientific areas under investigation.

the high-level mission requirements derived from our scientific objectives can be met at a number of locations at the lunar south pole.

6. Discussion and Perspectives

Our goal was to design a mission that is uniquely suited for the detection of water and other volatiles in the Moon's polar regions. Figure 9 gives an overview of the instruments we designed to achieve that goal. It also shows the primary areas of scientific interest and how the instruments provide complementary data on common objectives. The main strength of the mission's instrumentation is that every single instrument (the three primary ones plus the deployable units) contributes to the detection of water and hydrogen. The LCNS measures the hydrogen abundance to depths of about a meter or more, and can do so (with limited resolution) while the rover is in motion. The VCAS units can detect exospheric hydrogen and water released by thermal or mechanical disturbances of the regolith, either by natural or by artificial means, during the traverse and when they are deployed to locations of interest. While the rover is stationary, the VOILA instrument can detect hydrogen and water in the upper few millimeters of the regolith at concentrations of 0.5% by weight or less, and the LVS can sample the shallow subsurface for water ice with a sensitivity at least an order of magnitude better, to depths of about 15 cm, and also detect exospheric hydrogen and water.

This not only permits us to formulate an efficient operational concept, with the time-consuming sampling of the LVS mostly conducted at sites where an increased abundance of hydrogen was previously detected by the LCNS and VOILA instruments, it also allows for the combined analysis of instrument data, leading to an increased significance of our findings. This multi-instrument investigation is an important aspect that sets LUVMI-X apart from many other missions currently under development. It allows us to investigate not only the distribution of hydrogen, water, and other volatiles, but also their spatial and temporal migration process, which is likely driven by thermal perturbations due to illumination changes (Lucey et al. 2021). In addition, there are significant capability overlaps between the instruments in other areas: Both the VOILA and LCNS instruments will gather data on SWIPs and the composition of surface-layer regolith; the LVS and LCNS will both provide data on the composition of the regolith in the (shallow) subsurface; and the trio of VOILA, VCAS, and LVS will gather data on physisorbed volatiles in the surface layer. These capabilities are complemented by investigations each instrument can perform on its own: The LVS will gather data on subsurface, physisorbed volatiles; the VOILA instrument will determine the elemental composition of rocks and regolith along the rover's path; and the LCNS will characterize the radiation environment on the lunar surface. Altogether, these capabilities enable the comprehensive investigation of volatiles and surface chemistry in the polar regions of the Moon. The ability to deploy VCAS units into hard-to-reach places and remotely operate them adds further versatility and allows us to dynamically respond to the topology of the surveyed area.

Comparable capabilities are currently only foreseen with the Volatiles Investigating Polar Exploration Rover (VIPER), which will use a very similar set of instruments—a drill (TRIDENT), a mass spectrometer (MSolo), and a neutron spectrometer (NSS) (Ennico-Smith et al. 2020)—to search for water at depth, and an infrared spectrometer (NRVISS) to passively investigate the surface layer (Roush et al. 2021). Smaller rovers like MoonRanger will only carry a single instrument, in this case a neutron spectrometer, to detect water (Schweitzer et al. 2021), and therefore have relatively limited measurement capabilities. Instruments on static landers, such as the Package for Resource Observation and in Situ Prospecting for Exploration, Commercial exploitation and Transportation (PROSPECT)—formerly part of Luna 27 (Heather et al. 2021) and now likely to be launched on a commercial lander—will be able to assess the abundance of water and other volatiles in the immediate vicinity of the lander, but often only at very few locations within the range of a robotic arm. In addition to the obvious spatial limitations of such investigations, the contamination caused by the landers' thrusters may decisively limit the sensitivity to small abundances of volatiles in the surface layer.

On the level of individual instruments, the capabilities of the LVS are inferior to those of the drills of VIPER and PROSPECT, which both can reach depths of about 1 m and have more extensive and precise analysis capabilities. Its low mass, volume, and power consumption, however, make the LVS a good choice for mobile platforms that shall quickly survey large areas and primarily concentrate on ice in the shallow subsurface. The in situ heating capability and the coupling of the mass spectrometer to the sample volume provide operational and sensitivity advantages that facilitate faster and more direct sampling. In PROSPECT, samples must be transferred from the drill to another instrument for analysis (Sefton-Nash et al. 2018). While this rather complex operation allows the detailed investigation of samples from deep below the surface, it comes at the cost of increased system mass and power consumption, and is therefore impractical for a small rover that shall investigate a multitude of sites in as little as 14 days. It also bears a significant risk of losing or altering volatile content, due to thermal disturbances along the sampling chain (Mortimer et al. 2021). On VIPER, samples are not analyzed in a closed instrument; instead, they are observed by an infrared spectrometer after being lifted out of the drill hole (Ennico-Smith et al. 2020). In addition, volatiles sublimating off the samples are detected by a mass spectrometer mounted close to

the drill. Investigating samples in open system has the advantage that it is easier to use multiple independent instruments for analysis. The LVS, on the other hand, offers a more controlled environment with less potential for contamination by exospheric volatiles. Even though heating samples in situ has its own challenges and limitations (Biswas et al. 2020), overall the LVS design provides a measured balance between sensitivity, instrument size, and complexity for the investigation of volatiles on the surface and in the shallow subsurface.

The LIBS technique has been successfully used on the surface of Mars, most notably in the ChemCam and SuperCam instruments on the Mars Science Laboratory and Mars 2020 rovers, respectively (Maurice et al. 2016, 2021). The Tianwen-1 rover also carries an instrument that combines the technique with (passive) infrared spectroscopy (Zou et al. 2021). Using LIBS in the quasi-vacuum on the lunar surface presents unique challenges, as the lack of confining atmospheric pressure leads to the plasma dissipating more quickly. So far, the only instrument designed to explore the Moon was supposed to operate on the Chandrayaan-2 rover (Sundararajan 2018), which unfortunately never made it to the surface intact. The VOILA instrument is designed to be more capable than the instrument on Chandrayaan-2; its field of view, working distance, and resolution are, however, inferior to those of the larger and heavier ChemCam and SuperCam instruments operating on Mars. We are not aware of any other LIBS instrument for lunar exploration currently being under development, except for a possible reflight of the Indian system on Chandrayaan-3. Because of its higher complexity, successfully operating VOILA on the Moon would therefore be a technological first. An advantage of the LIBS technique is that it is operationally more versatile and can probe deeper than other techniques that analyze surface composition and volatiles from standoff distances (e.g., via infrared spectroscopy). This capability allows, for example, to determine the composition of rocks even when they are covered by a (thin) layer of regolith. The instrument is, however, technically and operationally more complicated, and it requires in situ calibration (Vaniman et al. 2012). Though VOILA can clearly distinguish between different minerals and rock types, it cannot achieve the sensitivities of a full-scale sample analysis suite.

Between the Apollo era and the landing of Chang'E 4 in 2019, no radiation measurements had been performed on the lunar surface. Investigations were performed in lunar orbit, for example by the CRaTER experiment on LRO (Spence et al. 2010), but the radiation environment on the lunar surface is believed to differ substantially from the one in orbit (Bhardwaj et al. 2015). The Lunar Lander Neutron and Dosimetry (LND) experiment on Chang'E 4 delivered the first measurement of the radiation field on the Moon, including a contribution of up to $23\% \pm 8\%$ by neutrons and gamma-rays (Zhang et al. 2020). Thanks to the sampling calorimeter at the heart of its telescope, the LCNS can measure charged particles over a much larger range of energy than LND, which essentially is a telescope of planar silicon detectors (Wimmer-Schweingruber et al. 2020). Though it is likely that other missions will carry radiation sensors of some form, only limited information about the instrumentation of many upcoming missions is available. The neutron spectrometer (NS) on Lunar Prospector (Feldman et al. 2004) and the Lunar Exploration Neutron Detector (LEND) on LRO (Mitrofanov et al. 2009) recorded global maps of the thermal and epithermal neutron fluxes from orbit using detectors based on ^{3}He gas proportional counters covered by different neutron-absorbing materials. Operating on the surface, the LCNS will inherently have a much higher spatial resolution, and it is designed to have a significantly increased energy resolution. LND, the only post-Apollo investigation to measure neutrons, is primarily sensitive to fast neutrons—and therefore has only a limited and experimental ability to measure the hydrogen abundance below the lander (Wimmer-Schweingruber et al. 2020). The MoonRanger (Schweitzer et al. 2021) and VIPER (Ennico-Smith et al. 2020) rovers will each carry a Neutron Spectrometer System (NSS), an updated but functionally equivalent derivative of the Lunar Prospector NS. The Neutron Measurements at the Lunar Surface (NMLS) instrument on Peregrine 1 (Fuqua Haviland et al. 2020) is based on the same measurement principle as the NSS, but it uses scintillator detectors instead of the more fragile gas proportional counters. The neutron-spectroscopy capabilities we aim to achieve with the LCNS are superior to those of both the NSS and NMLS instruments. The ability to simultaneously measure the charged-particle radiation environment also provides crucial data for interpreting neutron measurements.

Many recent discussions in the lunar-science community have revolved around ancient ice reservoirs suspected to exist several meters below the surface (Cannon et al. 2020), created primarily by water delivered through asteroid and comet impacts (Prem et al. 2015) or by volcanic outgassing from the lunar interior (Wilcoski et al. 2022). The simulations driving these discussions have not yet been verified experimentally, however, and their accuracy and predictive power may, according to their creators, suffer from several free and (partially) unknown parameters (Cannon & Britt 2020). The principal challenge is that most reservoirs are predicted to be buried so deeply that they can hardly be detected by any of the currently available technologies. The limited depths to which the LVS can sample and to which neutron spectroscopy can provide measurements mean that LUVMI-X will not be able to help shed light on the existence and extent of very deep reservoirs, though ice at depths up to about a meter could be detected by the LCNS. A recent analysis of multiple shadowed and illuminated craters similarly concluded that the smoothing of the surface inside polar craters may not be due to surface ice, but rather to larger deposits at depths that are inaccessible even to neutron spectroscopy and have therefore not been detected yet (Deutsch et al. 2021). Even though the LUVMI-X instruments cannot prove the existence of deep deposits, they are, at the very least, capable of testing the hypothesized absence of a correlation between surface ruggedness and surface ice.

An updated analysis of LRCOSS data, on the other hand, determined that a surface layer of dirty ice—i.e., water ice grains mixed with regolith, and an ice concentration that increases with depth—can best explain the amount of water (vapor) observed in the ejecta plume (Luchsinger et al. 2021). Even though the observations were not sensitive to the first few centimeters of material, and therefore cannot be used to determine the stratigraphy in the shallow subsurface, they seem to be consistent with either a layer of surface frost or older water ice covered with a thin layer of regolith. The LVS could test both hypotheses and therefore contribute to understanding the sources of water ice that accumulated in polar cold traps (Deutsch et al. 2020). Recent analytic models of impact

gardening show that, even if lunar water has a predominantly primordial origin, e.g., volcanic outgassing from the lunar interior (Wilcoski et al. 2022), deposits may be buried by as little as a few centimeters or by as much as several meters of regolith (Costello et al. 2020). The three instruments on LUVMI-X could either help to confirm the presence of shallow deposits down to depths of about a meter, or if they are absent, provide constraints for future models.

Both the LVS and VOILA are, in general, well suited to search for and quantify young (and possibly transient) surface frost that was detected from orbit in cold traps inside several permanently shadowed craters (Farrell et al. 2019). They could also investigate the near-surface stratigraphy of such deposits and search for ice at shallow depths. As both instruments are designed for comparatively fast sampling, they allow the time-resolved investigation of transient phenomena; the ability to point VOILA toward different targets while the rover is static also reduces operational complexity, as the vehicle does not need to move for every measurement. In addition, VCAS units could probe the suspected existence of an exospheric cloud of water molecules and icy grains above the floor of craters containing surface ice (Farrell et al. 2019). Both VCAS and the LVS can also investigate the thermally driven migration of volatiles, vertically and toward the poles (Reiss et al. 2021), by analyzing the upper surface layers and the lunar exosphere, in particular in locations with changing illumination conditions (Hendrix et al. 2019). Exospheric measurements during and after terminator events, e.g., observations of the thermally driven release of water or of its accumulation at dawn (Smolka & Reiss 2022), are key to the validation of simulated models of volatile migration.

SOFIA observations indicate that the widespread, low-level hydration of the lunar surface at high latitudes observed by infrared spectrometers from orbit (Clark 2009; Pieters et al. 2009; Sunshine et al. 2009) may be explained by water that is either confined inside impact glasses or trapped between regolith grains, though they do not allow these two possibilities to be distinguished (Honniball et al. 2021). LUVMI-X would be well suited to investigate which confinement mechanism is the dominant one: If water is trapped in the voids between grains, mechanically disturbing the surface would allow the molecules to be thermally liberated and subsequently be detected with the mass spectrometers in the LVS or in a VCAS unit. If water is predominantly trapped inside glasses, VOILA could reveal its presence there.

7. Conclusion

We are confident that its primary and secondary instruments and their capabilities render the LUVMI-X rover a unique and powerful tool for studying water and other volatiles on the Moon. Despite the limited depth to which its instruments can actively sample the lunar surface, the mission is nevertheless capable of addressing a wide range of open questions concerning the lunar water cycle—both regarding the origin of volatiles and their migration regionally as well as globally toward (polar) cold traps. And while it would certainly not be able to conclusively answer many of the questions by itself, it can complement—and in some areas enhance—the capabilities provided by other missions under development. The data gathered by LUVMI-X would also be highly relevant for some of these other investigations. Determining the contamination of the lunar surface in the vicinity of a lander equipped with thrusters, for example, would provide crucial context for the measurements of volatiles by instruments on static platforms like PROSPECT. Furthermore, maps of the hydrogen abundance in the mission area would provide detailed ground truth for past (e.g., Lunar Prospector, LRO) and future orbital measurements, such as those by LunaH-Map (Hardgrove et al. 2020), Lunar Flashlight (Cohen et al. 2020), and Lunar Trailblazer (Ehlmann et al. 2021).

To conclude with practical considerations relevant to future exploration efforts, we want to reiterate that ISRU—and especially the extraction of water and oxygen from the lunar regolith—promises to substantially decrease the amount of material that must be supplied to a permanently crewed outpost form Earth. It may also be essential for the development of near-Earth space and form the basis for a cis-lunar economy (Crawford 2015). Our current knowledge of the Moon's resource potential, however, is too incomplete to accurately assess the technical feasibility and economic viability of ISRU and other resource-extraction efforts. The LUVMI-X mission is well suited to help gather much-needed data about the availability, distribution, and accessibility of water and other volatiles on the Moon. Its unique instrumentation package sets it apart from other missions currently under development, because it will be able to provide complementary measurements by multiple instruments and investigate both the surface layer and the shallow subsurface. In addition, its ability to provide detailed measurements of both the charged and uncharged components of the lunar radiation environment is highly relevant to future crewed exploration missions. Our intent is to develop an affordable and adaptable system that not only provides scientifically interesting data to help shed light on open questions concerning the Moon's water and volatile cycle but also supports the development of lunar ice as a resource, which more than anything will require comprehensive in situ measurements by different missions and in multiple locations.

The LUVMI-X project received funding from the European Union's Horizon 2020 research and innovation program under grant agreement No. 822018. We thank Gen Ito from CRPG for fruitful discussions on the landing-site analysis, Patrick Wastian for his contributions to the LCNS design, Philipp Reiss for his help with improving the manuscript, and two anonymous reviewers for their valuable feedback.

ORCID iDs

Martin J. Losekamm https://orcid.org/0000-0001-7854-2334
Janos Biswas https://orcid.org/0000-0002-6150-665X
Matthieu Deremetz https://orcid.org/0000-0002-1239-0320
Jessica Flahaut https://orcid.org/0000-0002-0866-8086
Christian Gscheidle https://orcid.org/0000-0002-3939-1083
Thomas Pöschl https://orcid.org/0000-0003-3754-7221
Hannah M. Sargeant https://orcid.org/0000-0003-4987-5492
Susanne Schröder https://orcid.org/0000-0003-1870-3663
Simon Sheridan https://orcid.org/0000-0002-6059-6841
David S. Vogt https://orcid.org/0000-0003-1109-6960

References

Anand, M., Crawford, I. A., Balat-Pichelin, M., et al. 2012, P&SS, 74, 42
Anderton, R., Posselt, B., Komorowski, M., & Hodkinson, P. 2019, Occupational Medicine, 69, 311
Baiocco, G., Giraudo, M., Bocchini, L., et al. 2018, LSSR, 18, 1
Barker, M. K., Mazarico, E., Neumann, G. A., et al. 2021, P&SS, 203, 105119
Barnes, J. J., Kring, D. A., Tartese, R., et al. 2016, NatCo, 7, 11684
Bhardwaj, A., Dhanya, M. B., Alok, A., et al. 2015, GSL, 2, 10
Biswas, J., Sheridan, S., Pitcher, C., et al. 2020, P&SS, 181, 104826
Boynton, W. V. 2009, PDSS, Lunar Reconnaissance Orbiter Lunar Exploration Neutron Detector RDR Data V1.0,LRO-L-LEND-4/5-RDR-V1.0, doi:10.17189/1520636
Bramblett, R. L., Ewing, R. I., & Bonner, T. W. 1960, NucIM, 9, 1
Bussey, D. B. J., McGovern, J. A., Spudis, P. D., et al. 2010, Icar, 208, 558
Cannon, K. M., & Britt, D. T. 2020, Icar, 347, 113778
Cannon, K. M., Deutsch, A. N., Head, J. W., & Britt, D. T. 2020, GeoRL, 47, e88920
Chancellor, J. C., Blue, R. S., Cengel, K. A., et al. 2018, npjMG, 4, 8
Chyba, C., & Sagan, C. 1992, Natur, 355, 125
Clark, R. N. 2009, Sci, 326, 562
Cohen, B. A., Hayne, P. O., Greenhagen, B., et al. 2020, IAESM, 35, 46
Colaprete, A., Schultz, P., Heldmann, J., et al. 2010, Sci, 330, 463
Costello, E. S., Ghent, R. R., Hirabayashi, M., & Lucey, P. G. 2020, JGRE, 125, e06172
Crawford, I. A. 2015, PrPG, 39, 137
Crawford, I. A., Anand, M., Cockell, C. S., et al. 2012, P&SS, 74, 3
Crider, D. H., & Vondrak, R. R. 2002, AdSpR, 30, 1869
De Giacomo, A., & Hermann, J. 2017, JPhD, 50, 183002
Deutsch, A. N., Head, J. W., & Neumann, G. A. 2020, Icar, 336, 113455
Deutsch, A. N., Heldmann, J. L., Colaprete, A., Cannon, K. M., & Elphic, R. C. 2021, PSJ, 2, 213
Ehlmann, B. L., Klima, R. L., Bennett, C. L., et al. 2021, LPSC, 52, 1740
Elphic, R. C., Eke, V. R., Teodoro, L. F. A., Lawrence, D. J., & Bussey, D. B. J. 2007, GeoRL, 34, L13204
Ennico-Smith, K., Colaprete, A., Elphic, R., et al. 2020, LPSC, 51, 2898
Farrell, W. M., Hurley, D. M., Poston, M. J., et al. 2019, GeoRL, 46, 8680
Farrell, W. M., Hurley, D. M., & Zimmerman, M. I. 2015, GeoRL, 42, 3160
Fegley, B., & Swindle, T. D. 1993, in Resources of Near-Earth Space, ed. J. S. Lewis, M. S. Matthews, & M. L. Guerrieri (Tucson, AZ: Univ. Arizona Press), 367
Feldman, W. C., Ahola, K., Barraclough, B. L., et al. 2004, JGRE, 109, E07S06
Feldman, W. C., Maurice, S., Binder, A. B., et al. 1998, Sci, 281, 1496
Flahaut, J., Carpenter, J., Williams, J. P., et al. 2020, P&SS, 180, 104750
Fuqua Haviland, H., Bertone, P., Caffrey, J., Apple, J., & Team, N. 2020, LPSC, 51, 2935
Gläser, P., Oberst, J., Neumann, G. A., et al. 2018, P&SS, 162, 170
Granja, C., Polansky, S., Vykydal, Z., et al. 2016, P&SS, 125, 114
Green, R. O., Pieters, C., Mouroulis, P., et al. 2011, JGRE, 116, E00G19
Gruhn, C., Binimi, M., Legrain, R., et al. 1982, NIMPR, 196, 33
Hardgrove, C., Starr, R., Lazbin, I., et al. 2020, IAESM, 35, 54
Hayne, P. O., Aharonson, O., & Schörghofer, N. 2020, NatAs, 5, 169
Hayne, P. O., Hendrix, A., Sefton-Nash, E., et al. 2015, Icar, 255, 58
Heather, D., Sefton-Nash, E., Fisackerly, R., et al. 2021, EPSC, 15, 291
Hendrix, A. R., Hurley, D. M., Farrell, W. M., et al. 2019, GeoRL, 46, 2417
Hibbitts, C. A., Grieves, G. A., Poston, M. J., et al. 2011, Icar, 213, 64
Honniball, C. I., Lucey, P. G., Li, S., et al. 2021, NatAs, 5, 121
Kleinhenz, J., Smith, J., Roush, T., et al. 2018, in 16th Biennial Int. Conf. Engineering, Science, Construction, and Operations in Challenging Environments (Cleveland, OH: ASCE), doi:10.1061/9780784481899.044
Landis, M. E., Hayne, P. O., Williams, J.-P., Greenhagen, B. T., & Paige, D. A. 2022, PSJ, 3, 39
Lemelin, M., Blair, D. M., Roberts, C. E., et al. 2014, P&SS, 101, 149
Li, S., Lucey, P. G., Milliken, R. E., et al. 2018, PNAS, 115, 8907
Li, S., & Milliken, R. E. 2017, SciA, 3, e1701471
Lockheed Martin Corporation 2019, McCandless Lunar Lander User's Guide, https://www.lockheedmartin.com/en-us/products/mccandless-lunar-lander.html
Losekamm, M. J., Eckert, L., & Pöschl, T. 2022, in IEEE Aerospace Conf. (Piscataway, NJ: IEEE), 1
Lucey, P. G., Costello, E., Hurley, D. M., et al. 2020, LPSC, 51, 2319
Lucey, P. G., Petro, N., Hurley, D. M., et al. 2021, Geoch, in press
Luchsinger, K. M., Chanover, N. J., & Strycker, P. D. 2021, Icar, 354, 114089
Maurice, S., Clegg, S. M., Wiens, R. C., et al. 2016, J. Anal. At. Spectrom., 31, 863
Maurice, S., Wiens, R. C., Bernardi, P., et al. 2021, SSRv, 217, 47
Mazarico, E., Neumann, G. A., Smith, D. E., Zuber, M. T., & Torrence, M. H. 2011, Icar, 211, 1066
Meurisse, A., & Carpenter, J. 2020, P&SS, 182, 104853
Mitrofanov, I., Litvak, M., Sanin, A., et al. 2012, JGRE, 117, E00H27
Mitrofanov, I. G., Bartels, A., Bobrovnitsky, Y. I., et al. 2009, SSRv, 150, 183
Morse, A. D., Altwegg, K., Andrews, D. J., et al. 2012, P&SS, 66, 165
Mortimer, J. I., Abernethy, F. A. J., Barber, S. J., Reiss, P., & Heather, D. J. 2021, NASA Exploration Science Forum & European Lunar Symp. (USA: Solar System Exploration Research Virtual Institute)
Nozette, S., Lichtenberg, C. L., Spudis, P., et al. 1996, Sci, 274, 1495
Osinski, G. R., Cockell, C. S., Pontefract, A., & Sapers, H. M. 2020, AsBio, 20, 1121
Paige, D. A., Siegler, M. A., Zhang, J. A., et al. 2010, Sci, 330, 479
Peplowski, P. N., Beck, A. W., & Lawrence, D. J. 2016, JGRE, 121, 388
Pieters, C. M., Goswami, J. N., Clark, R. N., et al. 2009, Sci, 326, 568
Poston, M. J., Grieves, G. A., Aleksandrov, A. B., et al. 2013, JGRE, 118, 105
Prem, P., Artemieva, N. A., Goldstein, D. B., Varghese, P. L., & Trafton, L. M. 2015, Icar, 255, 148
Reiss, P., Warren, T., Sefton-Nash, E., & Trautner, R. 2021, JGRE, 126, e06742
Reitz, G., Berger, T., & Matthiae, D. 2012, P&SS, 74, 78
Richter, L., Deiml, M., Glier, M., et al. 2021, Proc. SPIE, 11852, 118521I
Robinson, M. S., Brylow, S. M., Tschimmel, M., et al. 2010, SSRv, 150, 81
Roush, T. L., Colaprete, A., Cook, A., et al. 2021, LPSC, 52, 1678
Schwadron, N., Wilson, J., Looper, M., et al. 2016, Icar, 273, 25
Schweitzer, L., Jamal, H., Jones, H., Wettergreen, D., & Red Whittaker, W. L. 2021, in 2021 IEEE Aerospace Conf. (50100) (Piscataway, NJ: IEEE), 1
Sefton-Nash, E., Carpenter, J. D., Fisackerly, R., & Trautner, R. 2018, LPSC, 49, 2740
Simpson, R. A., & Tyler, G. L. 1999, JGR, 104, 3845
Singleterry, R. C. 2013, AcAau, 91, 49
Smith, D. E., Zuber, M. T., Neumann, G. A., et al. 2017, Icar, 283, 70
Smolka, A., & Reiss, P. 2022, LPI Contribution, 2241, 5003, https://www.hou.usra.edu/meetings/lunarsurface17/pdf/5003.pdf
Spence, H. E., Case, A. W., Golightly, M. J., et al. 2010, SSRv, 150, 243
Speyerer, E. J., & Robinson, M. S. 2013, Icar, 222, 122
Speyerer, E. J., Robinson, M. S., Denevi, B. W., & Team, L. S. 2011, LPSC, 42, 2387
Stacy, N. J. S. 1997, Sci, 276, 1527
Stoffler, D., Ryder, G., Ivanov, B. A., et al. 2006, RvMG, 60, 519
Sundararajan, V. 2018, in AIAA Aerospace Sciences Meeting (Reston, VA: AIAA), 1
Sunshine, J. M., Farnham, T. L., Feaga, L. M., et al. 2009, Sci, 326, 565
Svetsov, V. V., & Shuvalov, V. V. 2015, P&SS, 117, 444
Vaniman, D., Dyar, M. D., Wiens, R., et al. 2012, SSRv, 170, 229
Wagner, R. V., Speyerer, E. J., Robinson, M. S., & Team, L. 2015, LPSC, 46, 1473
Wilcoski, A. X., Hayne, P. O., & Landis, M. E. 2022, PSJ, 3, 99
Williams, J. P., Greenhagen, B. T., Paige, D. A., et al. 2019, JGRE, 124, 2505
Williams, J. P., Paige, D. A., Greenhagen, B. T., & Sefton-Nash, E. 2017, Icar, 283, 300
Wimmer-Schweingruber, R. F., Yu, J., Böttcher, S. I., et al. 2020, SSRv, 216, 104
Wright, I. P., Sheridan, S., Barber, S. J., et al. 2015, Sci, 349, aab0673
Zhang, S., Wimmer-Schweingruber, R. F., Yu, J., et al. 2020, SciA, 6, eaaz1334
Zou, Y., Zhu, Y., Bai, Y., et al. 2021, AdSpR, 67, 812